Research Article

Mechanical Properties of Graphene Composite Materials and Mesonumerical Experiments on the Mechanical Properties of Unsaturated Soil-Rock Mixtures

Qinghai Zhang [iD],[1] Lihua Wu,[1] and Jianfei Li[2]

[1]*College of Agriculture and Hydraulic Engineering, Suihua University, Suihua, 152000 Heilongjiang, China*
[2]*Northeast Forestry University, School of Civil Engineering, Harbin, 150040 Heilongjiang, China*

Correspondence should be addressed to Qinghai Zhang; zqh464354668@163.com

Graphene, as an emerging two-dimensional carbon nanomaterial, has attracted widespread attention and in-depth research by domestic and foreign researchers. With its excellent mechanical properties, graphene is used as a reinforcing material in polymers, ceramics and rubber, and other matrices, which can significantly improve the toughness of the matrix. However, under the action of natural factors such as continuous rainfall or heavy rain, the accumulation layer landslide is often in an unsaturated state, which is very easy to induce disasters. Based on this background, we use micronumerical simulation methods and graphene composite materials to study the mechanical properties of unsaturated soil-rock mixtures to understand the mechanical properties of unsaturated soil-rock mixtures and evaluate and predict its stability. This paper takes the soil of a landslide zone in a certain city as the numerical test object. Through the automatic generation technology of the mesostructure model of the soil-rock mixture, a series of numerical experiments were carried out on the random mesostructure model of the soil-rock mixture, and the gravel content was analyzed in depth. Experiments show that the model can reasonably describe the volume expansion of the soil-rock mixture under low confining pressure, the volume compression under high confining pressure, and the phenomenon that the peak strength of the soil-rock mixture increases with the increase of confining pressure, which verifies that the model is simulating soil and rock. This shows that the stress-strain relationship curves of different soil-rock interface parameters, rock content, saturation, and the number of wet and dry cycles all show obvious nonlinear characteristics and strain hardening. This shows that graphene composites can be used in the study of the mechanics of unsaturated soil-rock mixtures, which is of great significance for improving the landslide environment and enhancing its mechanical properties.

1. Introduction

With the development of the national economy, in engineering practice, foundation resistance problems exist in UHV transmission line foundations, underground space foundations, high-rise building foundations, and marine construction foundations. Therefore, geotechnical scholars have more research on the resistance of foundations. More and more, it has gradually become a popular direction. In many engineering constructions, there are very high requirements

on the mechanical properties of soil-rock mixtures. Most of the natural shallow soils exist in unsaturated forms, with less overall water content, and have good shear resistance [1–3]. The increase of water content will weaken its performance, so the change of water content will have a greater impact on the mechanical characteristics of natural unsaturated soil. Of course, it is not the only influence. Therefore, the mechanical research on the properties of this kind of media, as well as the stability analysis, deformation and instability prediction, and prevention of the common accumulation

layer slopes and other slopes containing soil-rock mixed media in engineering construction in my country. It has good application value.

The rapid development of nanotechnology is continuously expanding the application of traditional materials such as soil and rock, bringing new opportunities and hopes to the development and transformation of mixed soil composite materials [4]. Nanomaterials are ultrafine materials with a particle size on the order of nanometers. Combining them with mixed soil can successfully enhance the mechanical strength of the mixed soil. Graphene, as a 2D layered inorganic nanomaterial with a periodic structure, is currently the strongest material known in the world [5, 6]. Due to its excellent mechanical properties, it can act in a polymer matrix like other nanomaterials, to nanoenhancement. At the same time, due to the physical properties of graphene itself, it can also be widely used in composite materials.

In the past ten years, scholars at home and abroad have conducted a large number of pioneering and fruitful researches on soil-rock mixtures and have accumulated rich research results and research experience. Qin et al. studied the preparation and mechanical properties of graphene and multiwalled carbon nanotube reinforced composite ceramic coatings. Use infrared spectroscopy (FTIR analysis) to identify the structure of functionalized and hybrid functionalized carbon nanotubes. The coating is brushed on the substrate and then cured at a temperature below 250°C. The morphological and cross-sectional features were studied by scanning electron microscopy (SEM). The experimental results show that the composite coating has a compact structure, and the graphene and the mixed-treated carbon nanotubes are well dispersed. The addition of 0.2 wt% graphene and 0.2 wt% hybrid functionalized carbon nanotubes resulted in a significant increase in hardness and fracture toughness. At the same time, due to the high tensile strength of graphene and carbon nanotubes, the bonding strength between the composite coating and the metal substrate is improved. Compared with pure alumina coating, the friction coefficient, wear depth, and wear width of composite coating are much lower. However, the experimental conclusions are not suitable for application to unsaturated soil-rock mixtures [7]. Lei et al. studied the characteristics of the shear strength parameters of the rock and soil aggregates in the embankment slope of the reservoir, gave the law of the shear strength of the rock and soil aggregates, and proposed the characteristics of the rock and soil aggregates considering the influence of suction and saturation. The unsaturated shear strength formula studies the physical mechanism of sliding or failure of such slopes under rainfall infiltration conditions. Based on the analysis of the slope rainfall infiltration process, a 3D unsaturated saturated-unsaturated seepage field and its finite element solution model were established. Studies have shown that the minimum safety factor of accumulated rock and soil aggregates is not reached when the rainfall stops, but occurs several hours after the rainfall stops. This phenomenon is consistent with the destruction process of the actual slope engineering, but its overall research lacks data support, and more data is needed to support its conclusions [8]. In order to obtain the mechanical properties of the weathered soil-rock mixture at the edge of a highway landslide in western China, Jin needed to perform large and medium-sized triaxial shearing on the three weathered rock-soil mixtures on site due to the reduction of sample size and particle size test. The effects of particle size and sample size were analyzed. The results show that it has a strong scale effect: mechanical properties are closely related to particle size, sample size, and sample classification. As the particle size increases, the internal friction angle increases first and then decreases. At the same time, the reasons for these differences are analyzed. The experimental results lack more data to support the trend of internal friction angle changes [8].

This paper uses the FORTRAN language program to realize the method of establishing the soil-rock mixture numerical model by the indoor test gradation, and with the help of the mesonumerical simulation method and the implicit integration algorithm, the finite element program is used to surround the seepage mechanics response of the soil-rock mixture of the accumulation layer landslide. And the mechanism of deformation and failure carries out a series of biaxial tests of unsaturated soil-rock mixed media under different soil-rock interface parameters, rock content, and saturation, and different numbers of dry and wet cycles, using soil mechanics, rock mechanics, seepage mechanics, and elastoplastic mechanics obtain the influence law of soil-rock interface parameters, rock content, saturation, number of dry-wet cycles, and other factors on the deformation and strength characteristics of soil-rock mixture to reveal its seepage mechanism and deformation and failure characteristics.

2. Mechanical Properties of Unsaturated Soil-Rock Mixture and Graphene Composite Materials

2.1. The Structure and Properties of Graphene. Since Professor N and Professor G successfully prepared single-layer graphene, graphene has attracted more and more attention and research from all walks of life. Graphene is the basic unit of other carbon materials in various dimensions. Currently, members of the carbon family include the following: zero-dimensional fullerenes, one-dimensional carbon nanotubes, and two-dimensional graphene to three-dimensional diamond and graphite. Graphene has a six-membered ring arranged in a periodic honeycomb structure, in which C atoms are connected to adjacent C atoms by sp^2 hybrid orbitals, the bond angle of the C-C bond is 120°, and the bond length is 0.142 nm. This stable structure gives graphene ultrahigh strength, with Young's modulus of 1.1 TPa and a breaking strength of 125 GPa. Each C atom of graphene has 4 valence electrons. When 3 electrons form an sp^2 bond, there will be an unbonded electron forming a large π bond above and below the plane of the graphene. At this time, the π bond is half-filled. The state allows electrons to move freely in it, and the large π bonds between layers form π orbitals perpendicular to the graphene plane. These π orbitals are effective channels for free electrons to shuttle

through the two-dimensional structure of graphene. Give graphene excellent electrical and thermal conductivity. The electron migration rate of graphene in a single atomic layer reaches $10000\,cm^2/v$, and the thermal conductivity is 3000-$5000\,wm^{-1}/k$. Theoretically, the specific surface area of a single-layer graphene can reach $2630\,cm^{-2}/g$, which not only further increases the electrical and thermal conductivity of graphene but also provides a larger contact area for its surface functionalization. In addition, the unique energy band structure of graphene also enables it to possess electromagnetic properties such as quantum Hall effect, quantum tunneling effect, and quantum Hall ferromagnetism. With its excellent properties in terms of force, light, electricity, and magnetism, graphene is widely used to enhance and improve the mechanical, electrical and electromagnetic shielding properties of composite materials.

Strictly speaking, there is thermodynamic instability in the two-dimensional crystal structure, and there is no long-range ordered two-dimensional crystal in nature. That is to say, if in a free state, the graphene sheet will curl into carbon nanotubes or stacked into graphite, which also makes graphene easy to agglomerate in a macroscopic state, and it is difficult to exist as a single layer.

Professor A added the original graphene and the functionalized graphene treated with nitric acid to the cement-based material to test its mechanical properties and explored the influence of the incorporation of graphene on calcium silicate hydrate. Atomic force microscope observations found that in cement-based materials mixed with graphene, graphene is present in the generated calcium silicate hydrate, and the content of high-density calcium silicate hydrate increases, and the overall mechanical properties of the composite material are enhanced. Molecular dynamics shows that the addition of functionalized graphene improves the interface strength and the integrity of cement-based composites. In addition, phase analysis shows that the incorporation of graphene and functionalized graphene can affect the phase composition and surface toughness of the product, which is the reason why the overall toughness and plasticity of graphene cement-based composites are improved.

2.2. Simulation Method of Soil-Rock Interface.

In a soil-rock mixture, the existence of soil-rock interface has an important influence on its mechanical properties and deformation and failure characteristics [9, 10]. The contact of the soil-rock interface is a typical nonlinear problem. In the numerical calculation, the contact surface element is generally introduced to simulate the contact problem. When there are many contact surfaces, the calculation is often not easy to converge [11, 12]. Therefore, for materials with a large number of discontinuous surfaces on the mesoscale, such as soil-rock mixture, the use of conventional contact surface elements to simulate the soil-rock interface has obvious limitations.

2.2.1. Master-Slave Interface Model.

The master control plane can invade the slave plane between the nodes of the slave plane, as shown in Figure 1(a) [13]. This regulation can well realize the simulation of the mechanical behavior of the soil-rock interface, because in the soil-rock mixture, the stiffness and strength of the rock are generally much greater than those of the soil, and the rotation and translation of the rock under the external load will affect it. The surrounding soil produces contact force, and the sharp corners of the rock passing through the soil will cause the deformation and failure of the soil, which is consistent with the mechanical mechanism of the interaction between soil and rock [14, 15].

In order to obtain the best simulation results, when simulating the soil-rock interface, the pair of surfaces in contact between the rock and the soil is defined as the contact pair in the calculation model. The soil surface is the subordinate contact surface, and the rock surface is the dominant contact surface shown in Figure 1(b) [16].

2.2.2. Friction Model.

When simulating the contact characteristics of soil and boulders, the Coulomb friction model should be used as the soil-rock interface contact model, and the friction factor is used to characterize the friction behavior between two surfaces. The relationship between stress and shear displacement on the contact surface is shown in Figure 2.

The solid line in the figure is the ideal friction behavior. The default friction factor is 0 (the contact surface is completely smooth). Before the stress at the contact surface reaches the maximum stress τ_{max}, the tangential slip is 0 until the stress between the contact surfaces is equal to the relative sliding of the contact surface which will occur only when the ultimate stress μp is [17, 18], namely,

$$\tau_{max} = \mu p. \tag{1}$$

In the formula, μ is the friction factor, and p is the normal contact force between the two contact surfaces.

2.3. Unsaturated Soil Seepage and Strength

2.3.1. Unsaturated Seepage.

The flow of liquid pores into unsaturated soils follows Darcy's law or Forchheimer's law, and the expressions are as follows:

$$V = -K\,grad H = KJ, \tag{2}$$

$$snV_f\left(1 + \beta\sqrt{V_f \cdot V_f}\right) = -K\frac{\partial H}{\partial X} = -K\,grad H, \tag{3}$$

where V is the seepage velocity, J is the hydraulic gradient, H is the piezometric head, snV_f is the seepage velocity through the unit area in a certain direction, and K is the permeability coefficient [19, 20].

According to Darcy's law, there are

$$k = \frac{v}{gK}. \tag{4}$$

According to Forchheimer's law, there are

$$k = \frac{v}{g + g\beta\sqrt{V_f \cdot V_f}}K. \tag{5}$$

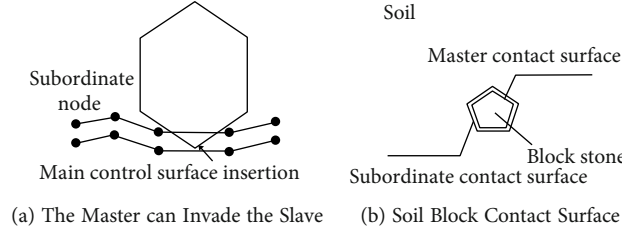(a) The Master can Invade the Slave   (b) Soil Block Contact Surface

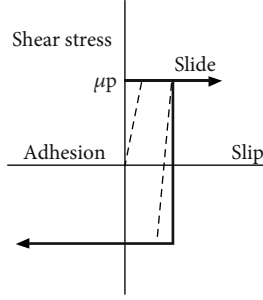FIGURE 1: Simulation method of soil-rock interface.

FIGURE 2: Schematic diagram of Coulomb friction model.

In the formula, v is the dynamic viscosity coefficient. For unsaturated soil, since liquid and gas coexist, the degree of saturation directly affects the permeability resistance, so at this time, k or K is a function of the degree of saturation S, so it is uniformly written as

$$k = k_s(S)K. \tag{6}$$

In the formula, $k_s(S)$ is the saturation correlation coefficient, and for isotropic materials, K is a scalar.

2.3.2. Unsaturated Soil Strength. An important factor in the instability of the soil-rock mixture slope caused by rainfall is that the rainfall causes the reduction of the matrix suction in the shallow unsaturated soil-rock mixture, resulting in loss [21, 22]. The influence of unsaturated characteristics on soil-rock mixture is mainly reflected in the influence of matrix suction on its shear strength, namely,

$$\tau_f = c' + (\sigma - u_a)\tan\phi' + (u_a - u_w)\tan\phi^b. \tag{7}$$

In the formula, τ_f is the shear strength of unsaturated soil, σ is the normal stress, and $\sigma - u_a$ is the net normal stress.

2.4. Automatic Generation Technology of Soil-Rock Mixture. With the rapid development of digital graphics processing technology, remarkable results have also been achieved in the mesostructure of soil-rock mixtures. However, digital image processing technology largely relies on the acquired cross-sectional images of all the soil-rock mixtures in the study area, so this method has certain limitations [23–26]. The main function of the preprocessing program of the soil-rock mixture numerical model is to generate a certain amount of rock in a specific research area, so that the parti-

cle size distribution of the rock system itself conforms to a specific gradation curve. Furthermore, it is possible to make the generated discrete stone system have statistical self-similarity properties, that is, fractal [27].

2.4.1. Random Number. The stochastic simulation method is used to simulate the size, orientation and spatial distribution of the blocks in the soil-rock mixture, namely,

$$R_i = \text{mod}\,(2053R_{i-1} + 13849, m), \tag{8}$$

$$\text{RND}_i = \frac{R_i}{m}. \tag{9}$$

Among them, R_{i-1} is the seed number that triggers the random number generator input from the outside.

2.4.2. The Shape of the Block Stone in the Soil-Rock Mixture. In order to simulate boulders objectively, arbitrary random polygons are used in the program to simulate boulders. The maximum and minimum number of sides of the boulders is put from the outside [28]; then,

$$L(x, \lambda) = f(x) - \lambda^T c(x). \tag{10}$$

Among them,

$$c((x)) = (c_1(x), \cdots, c_p(x))^T, \tag{11}$$

$$\varphi(x, u) \equiv f(x) + \frac{1}{\mu}\|c(x)\|_1. \tag{12}$$

Among them, μ is called the penalty factor, and $\|c(x)\|_1$ is the l_1 norm of the vector function $c(x) = (c_1(x), \cdots, c_p(x))^T$. In the specific simulation process, as needed, the concave polygon is not needed for artificial control [29, 30].

2.4.3. Determination of the Spatial Position and Orientation of Block Stones in Soil-Rock Mixture. First, create the center of the rock, and then multiply the random number by the width of the sample to get the coordinate value of the center of the rock in the sample [31, 32]. Before determining the vertex coordinates of the polygon, a random number must first be created as the angle of deflection of the side of the polygon. After determining the deflection angle, since the number of sides of the polygon has been determined, the deflection angle required to generate a polygon radius can

be calculated as

$$\beta = a + (i - 1) \cdot \frac{2\pi}{n}.$$ (13)

Then, generate a random number and combine the boundary diameter of the polygon with the maximum and minimum radius to determine the radius of the polygon at this time. After the polygon radius is determined, since the angle between the polygon side and the *x*-axis is known, multiply the angle by the angle. The cosine and sine values of can get the vertex coordinates of the polygon [33, 34].

2.4.4. Determination of the Area of Block Stone in Soil-Rock Mixture. This type of polygon is decomposed into multiple triangles, and the area of the polygon is calculated by calculating the area of the triangle separately. The formula used is as follows:

$$\text{Area} = \frac{1}{2} \sum_{i=1}^{n} \begin{vmatrix} x_0 & x(i) & x(i+1) \\ y_0 & y(i) & y(i+1) \\ 1 & 1 & 1 \end{vmatrix}.$$ (14)

Among them, (x_0, y_0) is the coordinate of the center of the polygon; $(x(i), y(i))$ is the coordinate of the vertices of the polygon.

2.4.5. Determination of rock content in the model. In the established two-dimensional model, the size of the stone content is defined as the ratio of the area occupied by the boulders in the model to the total area of the model. The specific formula is as follows:

$$e = \frac{\sum A_i}{A}.$$ (15)

In the formula, *e* is the stone content rate, A_i is the area of a single stone, and *A* is the total area of the model.

2.5. Mechanical Safety of Unsaturated Soil-Rock Mixture. Since the mechanical properties of the unsaturated soil-rock mixture effectively inherit the advantages of steel and concrete, it has good plasticity and adjustability and can form a beautiful structure. It has high strength and rigidity and can be built into a larger span structure. Good integrity, good ductility, and the structure can better resist external disasters, such as earthquakes and hurricanes; good durability and fire resistance can be applied to many characteristics such as harsh environments and widely used in construction and other civil engineering.

3. Experimental Design of Mechanical Properties of Unsaturated Soil-Rock Mixture

3.1. Test Subject. Taking the landslide zone soil in a landslide area of this city as the object of numerical experiment, through the automatic generation technology of the mesostructure model of the soil-rock mixture, a series of numerical experiments were carried out on the random mesostructure

model of the soil-rock mixture, and the gravel content, the soil-rock contact characteristics, saturation, dry-wet cycle, and many other factors affect the macromechanical properties and deformation failure of unsaturated soil-rock mixtures. The material composition of the landslide accumulation body and the sampling point diagram of the accumulation body are shown in Figure 3.

3.2. Content of Numerical Experiment

3.2.1. Mechanical Properties of Unsaturated Soil-Rock Mixture under Different Rock Contents. The unsaturated soil-rock mixture consists of soil and crushed stone. The different content of crushed stone will change the internal structure of the soil-rock mixture, which will inevitably affect its mechanical deformation properties. Based on the landslide zone test ground gradient in a landslide-prone area of this city, the random soil-rock mixture intermediate generation system is used to create numerical experimental geometric models with different rock contents and the corresponding unsaturated soil-rock mixture. They are determined in the ABAQUS test model, perform a biaxial compression test, and study the effect of the content of crushed rocks on the stress-stress ratio and volume-axial stress curve of the unsaturated soil-rock mixture.

3.2.2. Mechanical Properties of Unsaturated Soil-Rock Mixtures under Different Saturations. As a typical heterogeneous bulk material, unsaturated soil-rock mixture has a large internal porosity and is affected by saturation. This paper uses the ABAQUS program as a platform to combine mechanical calculations and seepage calculations to conduct biaxial tests of unsaturated soil-rock mixture samples under different saturation conditions. Study the mechanical properties and failure mechanism of soil-rock mixture samples under different saturations.

3.3. Numerical Test Model Establishment. The numerical test refers to the indoor triaxial shear test of a sliding body in a landslide area in this city for sample preparation. The indoor test is scaled according to the original gradation of the sliding body at the landslide site. The particle size of the sample is above 60 mm, accounting for 5.22%. The particle size of 20 mm or more accounts for 25.52%, and the content of fine particles smaller than 5 mm is 35.84%. Therefore, the equivalent replacement method is used to scale the ultraparticle size part, and the ultraparticle size part ($d_{\max} = 60$ mm) is 60-5 mm. Perform equivalent substitutions, and the gradation composition is shown in Table 1.

3.3.1. Determination of Minimum Particle Size. This frequency value test adopts a 30 cm * 60 cm biaxial test. The minimum particle size of the numerical biaxial test is determined by the soil-rock threshold combined with the original gradation of the landslide body to be 1 cm.

3.3.2. Model Establishment. This paper simulates the five sets of gradation curves of the indoor triaxial test. Within the range of 30 cm * 60 cm, the self-developed random stone generation system is used to automatically generate crushed

Material composition of
deposits before landslide

Material composition of
deposits after landslide

Exposed section of bedrock
and accumulation body
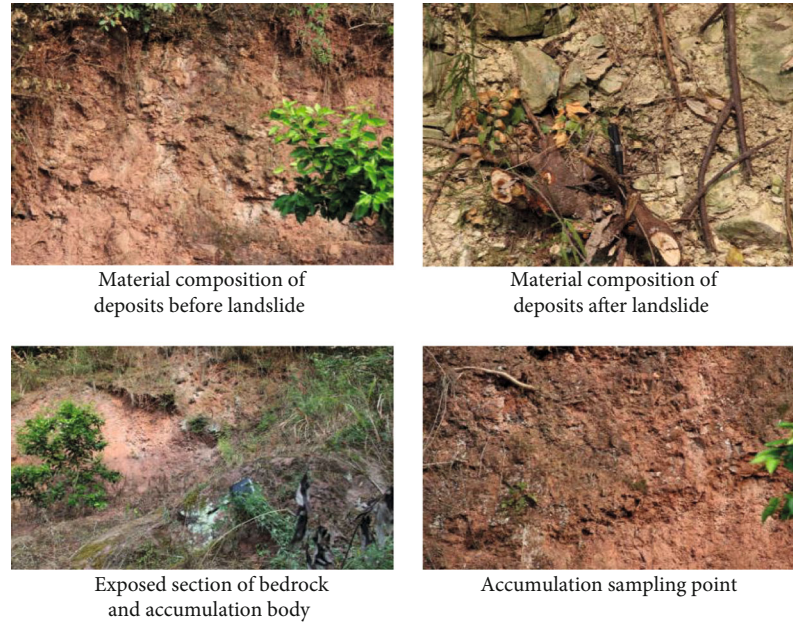

Accumulation sampling point

FIGURE 3: Material composition of the landslide accumulation body and the sampling point map of the accumulation body.

TABLE 1: Test grading of rock and soil slide.

| Test gradation | Percentage of each granule group | | | | | | | | | |
| | 60-40 | 40-20 | 20-10 | 10-5 | 5-2 | 2-1 | 1-0.5 | 0.5-0.25 | 0.25-0.1 | <0.1 |
						(mm)				
1	0	0	20.18	21.41	15.60	8.41	8.67	6.35	6.05	10.32
2	0	13.50	24.20	19.30	12.50	8.80	7.20	3.70	3.70	7.10
3	5.27	17.43	26.19	16.23	10.79	7.56	5.82	2.68	2.76	5.27
4	8.50	22.50	25.00	17.00	9.00	6.00	4.00	3.00	3.00	1.00
5	15.76	26.83	23.55	14.32	9.43	3.36	4.56	2.19	0	0

stones and soil, and then, the corresponding nonstandards are established in ABAQUS.

3.3.3. Crushed Stone Content.
According to the grading curve, the rock content is 32%, 38%, 47%, 56%, and 65%, and then, the geometric model of the soil-rock mixture is generated according to the random generation system of the block stone, and the corresponding geometric model is established in ABAQUS. Divide the grid, as shown in Figure 4, and set the initial conditions and boundary conditions of the soil-rock contact characteristics of the unsaturated soil-rock mixture to prepare for the next biaxial numerical test.

3.4. Statistical Processing.
Statistical analysis was performed with SPSS 13.0 statistical software. The significance test of the difference was performed by one-way analysis of variance, the difference between the two groups was tested by LSD-t, and the statistical results of the mechanical properties of the unsaturated soil-rock mixture were performed by the group t-test. $P < 0.05$ is considered to be statistically significant.

4. Mechanical Properties of Unsaturated Soil-Rock Mixture

4.1. Verification of Numerical Model Test.
Take the indoor triaxial test of gravel soil with 47% gravel content as an example to verify the rationality of the random soil-rock mixture model. The parameters of the biaxial numerical model are shown in Table 2.

The size of the model is 30 cm ∗ 60 cm from the previous three-axis test. The vertical displacement of the bottom boundary is constrained, the surrounding stress boundary conditions are used, and the top of the model is servo controlled to apply axial load. Confining pressures of 0.4 MPa, 0.8 MPa, 1.2 MPa, and 1.6 MPa were, respectively, applied in the calculation of the biaxial test. The calculation results of the biaxial test mainly analyze the relationship between deviatoric stress and axial strain and the relationship between volume and axial strain. At the same time, it is compared with the indoor test results, as shown in Figures 5 and 6.

Figures 5 and 6 show that the normality of the calculated value of the model and the measured value of the test are the same whether it is the voltage-voltage ratio curve or the

Stone content 32% Stone content 38% Stone content 47% Stone content 56% Stone content 65%
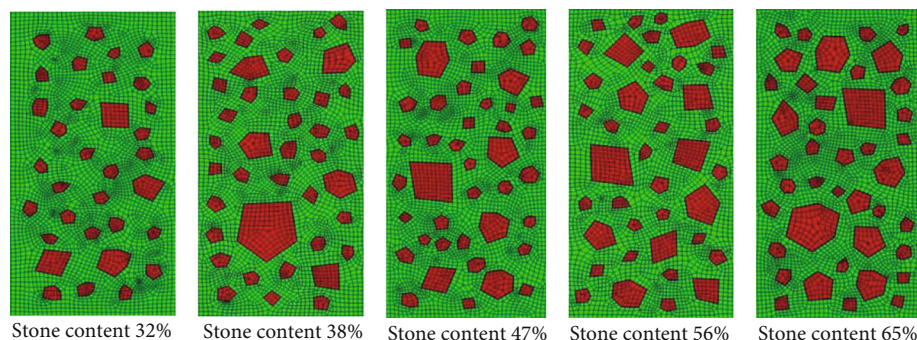
FIGURE 4: Soil-rock mixture samples of different rock block contents in FEM.

TABLE 2: Table of physical and mechanical parameters of soil-rock mixture test.

Material type	Density (kg·m^{-3})	Elastic modulus (MPa)	Poisson's ratio	Internal friction angle (°)	Cohesion (kPa)
Clod	2000	50	0.38	28	50
Block stone	2800	17500	0.20	41	12000

volume-axis voltage ratio curve, which shows the adaptability of the model to different pressure situations. It shows that the model can reasonably describe the volume expansion of the soil-soil mixture at low constraint pressure, the compression of the volume under high constraint pressure, and the increase of the maximum strength of the soil-rock mixture with the increase of the constraint pressure, which confirms that the model simulates a soil-rock mixture.

4.2. Deformation Characteristics of Unsaturated Soil-Rock Mixture under Different Soil-Rock Interface Parameters. Using the unsaturated numerical test model, the biaxial consolidation drainage test was carried out under the confining pressure of 0.4 MPa, 0.8 MPa, 1.2 MPa, and 1.6 MPa, respectively. During the loading process, the confining pressure is kept stable by the strain servo control, and the speed of the upper loading plate is controlled to apply the axial force to obtain the stress-strain relationship curve and the volume-axial strain relationship curve of the corresponding confining pressure under different soil-rock interface contact parameters, such as shown in Figures 7 and 8.

It can be seen from Figures 7 and 8 that the stress-strain relationship curves of the unsaturated soil-rock mixture with the same rock content show obvious nonlinear characteristics. The initial linear segments coincide, and the peak principal stress difference increases with the increase of confining pressure. The five types of samples with rock content all show the characteristics of strain hardening, and with the increase of confining pressure, the phenomenon of strain hardening becomes more significant. From the volumetric strain-axial strain relationship curve, it can be seen that at low confining pressure, the specimens have undergone a deformation process from shear shrinkage to dilatancy. As the confining pressure increases, the dilatancy

deformation of the specimen gradually weakens at high confining pressure. During compression, the specimen basically exhibits shear deformation, and with the increase of strain, the growth rate of shear deformation tends to decrease. Under the same confining pressure, the larger the rock content of the unsaturated soil-rock mixture, the higher the peak strength value. The smaller the axial strain when the peak strength is reached, the more rock content and the greater the initial elastic modulus of the sample, which will enter the plasticity. After the deformation stage, the strain hardening characteristics are more pronounced.

4.3. Failure Mechanism of Unsaturated Soil-Rock Mixture under Different Soil-Rock Interface Parameters. Under various soil-rock interface parameters, the mesoscopic failure morphology of each sample during each axial strain process under confining pressure is shown in Figure 9.

It can be seen from Figure 9 that when the friction coefficient of the soil-rock interface is small, the unsaturated soil-rock mixture appears as a loose failure mode, with obvious open cracks, and when the friction coefficient is large, it appears as an overall failure. This is due to the broken stones and the soil. During the loading process, the gravel inside the soil-rock mixture moves and rotates. When there is no friction between the soil and the boulder or the friction is small, the movement of the boulder cannot drive the surrounding soil. The coordinated deformation of the body will leave a large gap behind it. When the soil behind it reaches a plastic state, the crushed stones can not play a restraint, making the shear failure zone of the soil-rock mixture extremely irregular and appearing to be circumscribed. When the interface friction coefficient is very large, the greater the occlusion between the rock and the surrounding soil, the more coordinated the deformation of the rock and the surrounding soil; the friction required for basic rotation and translation of the rock is very large, so only translation and dislocation occur. So the shear failure zone basically passes through the sharp corners of the rubble and seldom branches and bypasses the previous rubble.

4.4. Mesopermeability Test Analysis. In order to study the influence of the rock content of the soil-rock mixture on the macroscopic permeability, the test selects the rock content of 32%, 38%, 47%, 56%, and 65% and five conditions, respectively. When the crushed stone is in close contact with
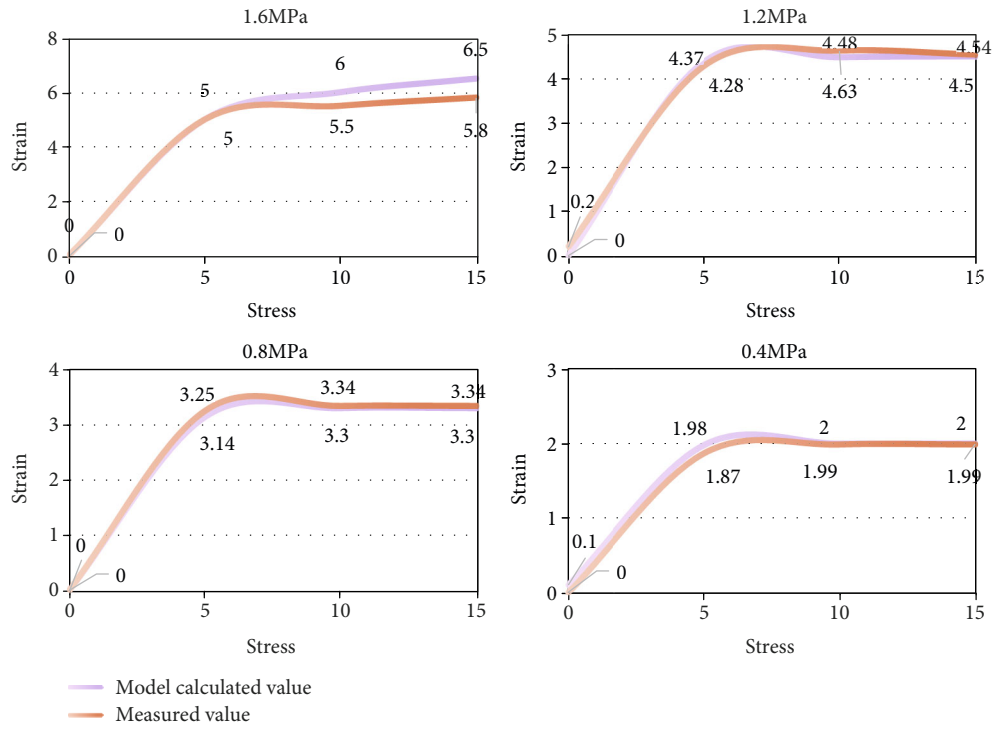
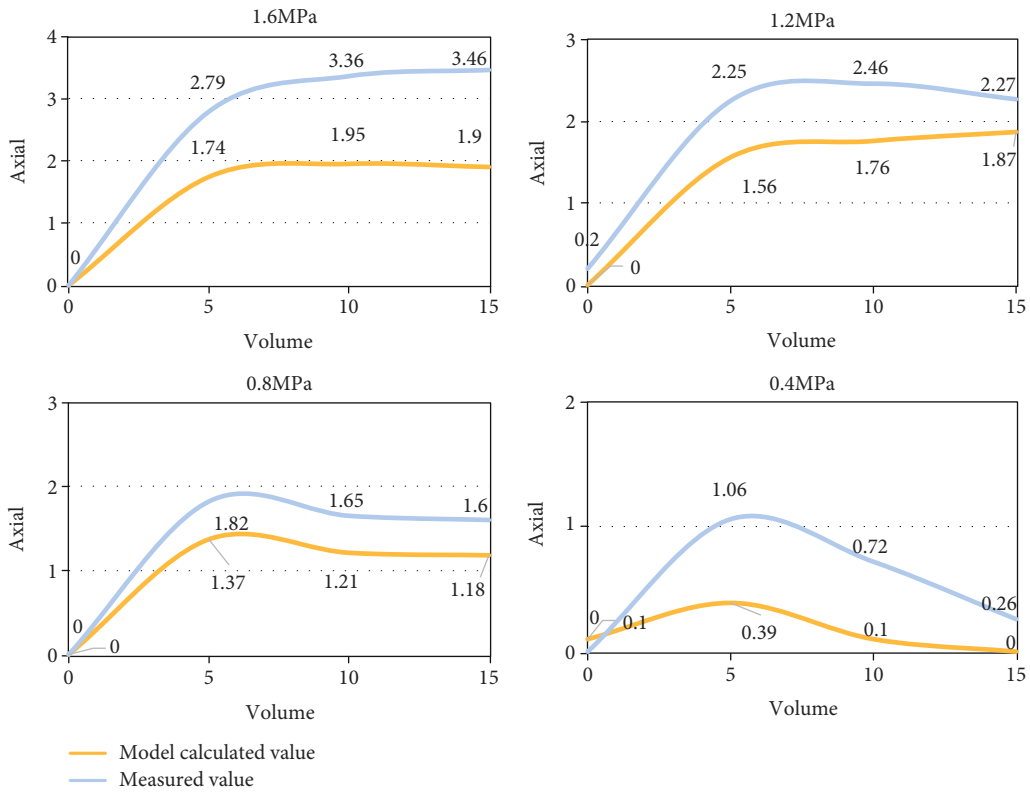Figure 5: Stress-strain relationship curve.

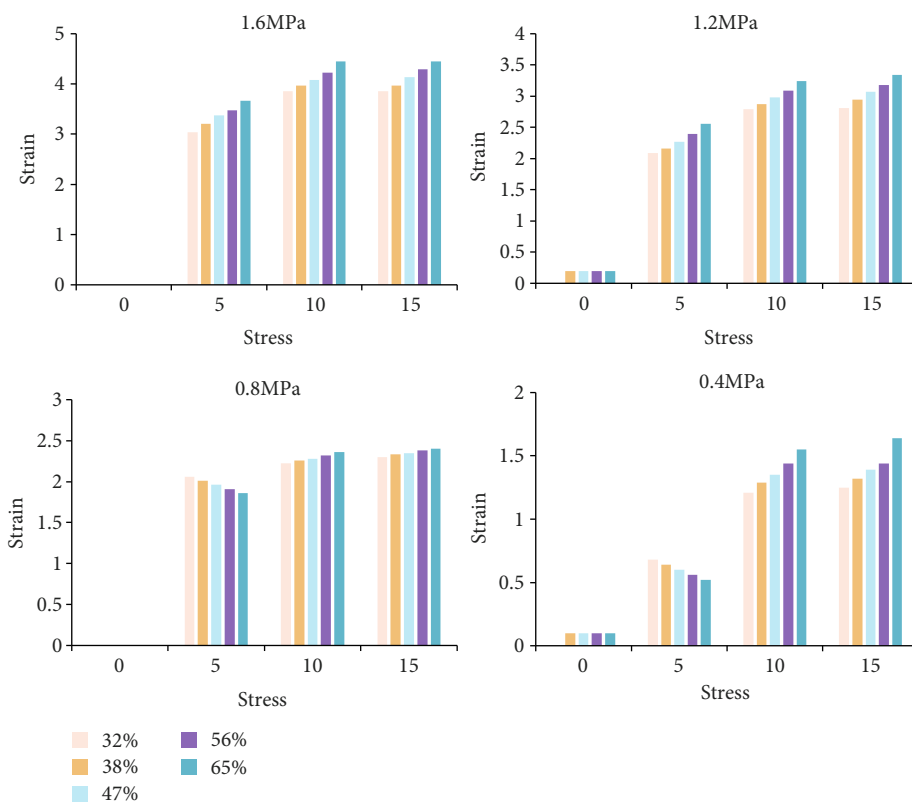Figure 6: Volume-axial strain relation curve.

Figure 7: Stress-strain relationship curve of different rock content under the same confining pressure.
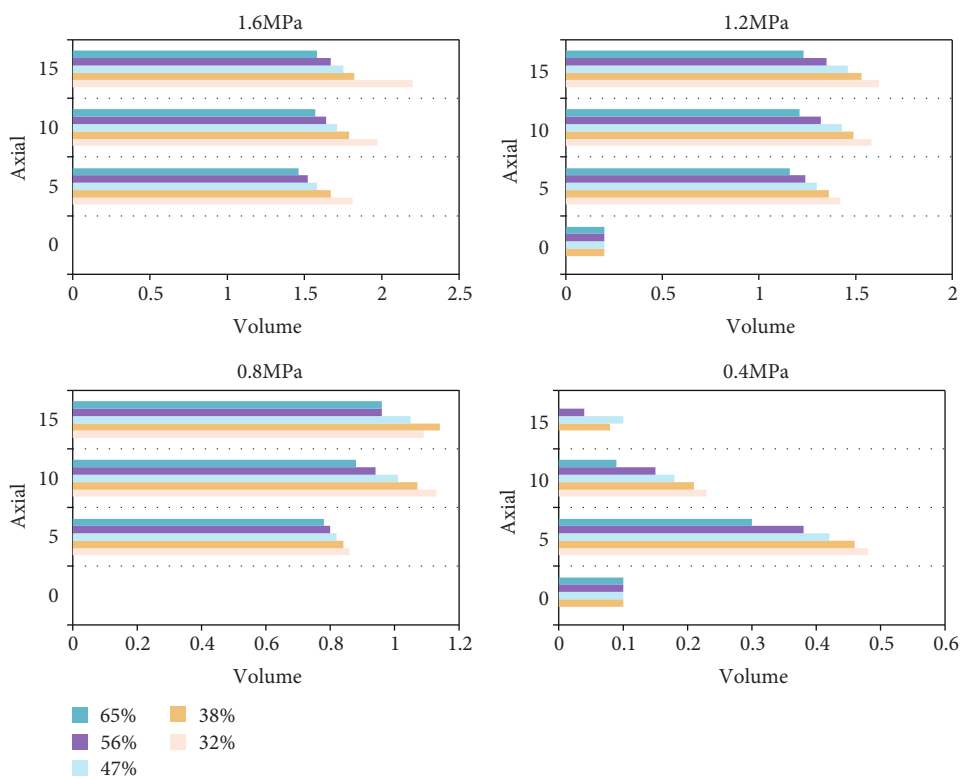

Figure 8: Volume-axial strain curve of different rock content under the same confining pressure.
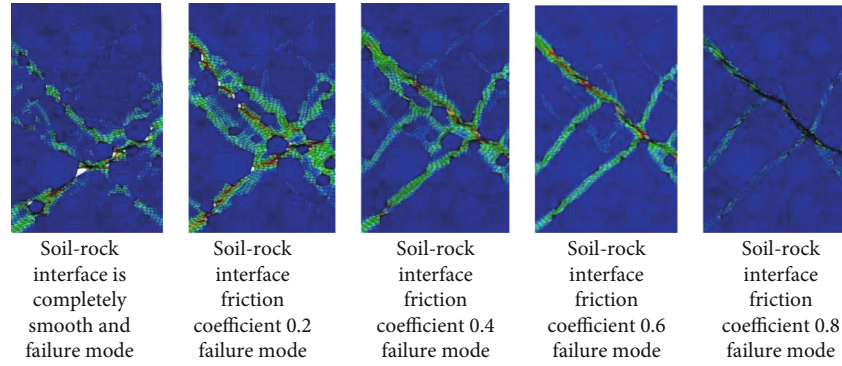
| Soil-rock interface is completely smooth and failure mode | Soil-rock interface friction coefficient 0.2 failure mode | Soil-rock interface friction coefficient 0.4 failure mode | Soil-rock interface friction coefficient 0.6 failure mode | Soil-rock interface friction coefficient 0.8 failure mode |

FIGURE 9: Final failure form of unsaturated soil-rock mixture.
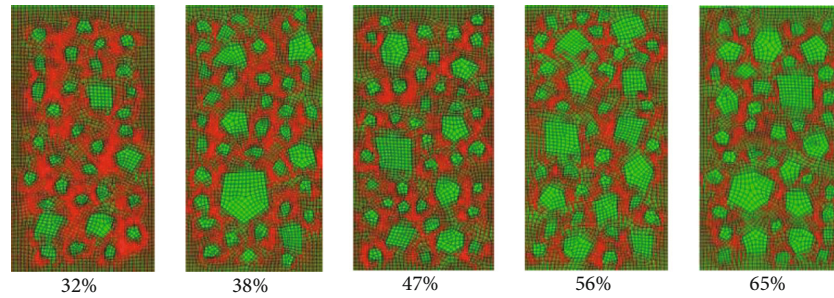

| 32% | 38% | 47% | 56% | 65% |

FIGURE 10: Characteristics of mesolevel seepage field of unsaturated soil-rock mixture with different rock content.

TABLE 3: Relationship curve between permeability coefficient and rock content of unsaturated soil-rock.

Osmotic pressure (MPa)	0	20	40	60	80
0.1	0.095	0.082	0.078	0.074	0.069
0.2	0.098	0.087	0.085	0.083	0.080
0.3	0.101	0.095	0.098	0.101	0.103
0.4	0.105	0.107	0.118	0.129	0.139

the soil and the permeability of the stone is not considered, the mesoseepage field distribution of each sample obtained through the numerical permeability test is shown in Figure 10.

According to the results of numerical experiment analysis, the relationship between the macropermeability coefficient of the soil-rock mixture and the rock content of the soil-rock mixture is drawn as the ordinate. The results are shown in Table 3.

It can be seen from Table 3 that the macroscopic permeability coefficient of soil-rock mixture changes with rock content obtained from the prediction of each mesostructure model and numerical experiment. It can be seen that when the rock is in close contact with the soil, when the pore water passes through the broken rock in the narrow soil between the rocks, the seepage rate is relatively large, and the pore water pressure contours are densely distributed. The pore water pressure of these parts on the surface drops faster. The narrower the channel, the denser the value, and the faster the pore water pressure drops. The permeability before and after the block rock is very small. Under the same seep-

age pressure, the macroscopic permeability coefficient of the unsaturated soil-rock mixture decreases with the increase of the rock content. This is mainly because the pore water flows through the pores in the unsaturated soil between the crushed stones. The increase in the rock content of the soil and the narrowing of the spacing between the crushed stones makes the soil more discontinuous, and the flow of pore water is more difficult.

5. Conclusions

In this paper, the purity, crystallinity, chemical structure, and micromorphology of graphene are characterized and analyzed at multiple levels through comprehensive testing methods such as microscopy, providing a reliable basis and basic guarantee for subsequent testing. Based on the random rock generation system, the corresponding unsaturated soil-rock mixture ABAQUS finite element program was compiled. Using the master-slave contact algorithm, the characteristics of the soil-rock interface, rock content, saturation, and dry humidity were proposed. After fusing the graphene composite material into the unsaturated soil-rock mixture, starting from the difference in circulation, the biaxial numerical test method is used to deeply analyze the influence of various factors such as soil-rock interface parameters, rock content, saturation, and dry and wet cycles. Study its mechanical properties and the microscopic damage mechanism and macroscopic mechanical behavior of unsaturated soil-rock mixtures. From the shape of the stress-strain relationship curve, the stress-strain relationship curves of different soil-rock interface parameters, rock

content, saturation, and the number of wet and dry cycles all show obvious nonlinear characteristics and strain hardening. As the confining pressure increases, the hardening becomes more obvious. The shear strength parameters of unsaturated soil-rock mixtures increase with the increase of soil-rock interface parameters. Finally, there is a comprehensive use of various microtesting methods to study the microscopic mechanism of graphene in the soil-rock mixture. When the soil-rock interface is completely smooth, the unsaturated soil-rock mixture sample is broken in bulk, with obvious open cracks and obvious dilatancy. When the interface parameter increases to a certain extent, the unsaturated soil-rock mixture is destroyed as a whole, and the dilatancy phenomenon is not very obvious. Both the constitutive model and the yield criterion of the numerical experiment in this paper adopt the Mohr Coulomb model, which has a certain gap with the results of the indoor experiment. Therefore, it is necessary to strengthen the theoretical research.

Data Availability

The data that support the findings of this study are available from the corresponding author upon reasonable request.

Conflicts of Interest

The authors declared no potential conflicts of interest with respect to the research, authorship, and/or publication of this article.

Acknowledgments

References

[1] S.-B. Tsai, R. Saito, Y.-C. Lin, Q. Chen, and J. Zhou, "Discussing measurement criteria and competitive strategies of green suppliers from a green law perspective," *Proceedings of the Institution of Mechanical Engineers, Part B: Journal of Engineering Manufacture*, vol. 229, 1_suppl, pp. 135–145, 2015.

[2] S.-B. Tsai, Y.-C. Lee, and J.-J. Guo, "Using modified grey forecasting models to forecast the growth trends of green materials," *Proceedings of the Institution of Mechanical Engineers, Part B: Journal of Engineering Manufacture*, vol. 228, no. 6, pp. 931–940, 2014.

[3] S. B. Tsai, Y. Z. Xue, P. Y. Huang et al., "Establishing a criteria system for green production," *Proceedings of the Institution of Mechanical Engineers, Part B: Journal of Engineering Manufacture*, vol. 229, no. 8, pp. 1395–1406, 2014.

[4] Y. Tang, Z. Chen, W. Feng, Y. Nong, C. Li, and J. Chen, "Combined effects of nano-silica and silica fume on the mechanical behavior of recycled aggregate concrete," *Nanotechnology Reviews*, vol. 10, no. 1, pp. 819–838, 2021.

[5] P. Wang, T. Yao, Z. Li et al., "A superhydrophobic/electrothermal synergistically anti-icing strategy based on graphene composite," *Composites Science and Technology*, vol. 198, article 108307, 2020.

[6] L. Zeng, J. Shi, J. Luo, and H. Chen, "Silver sulfide anchored on reduced graphene oxide as a high -performance catalyst for CO_2 electroreduction," *Journal of Power Sources*, vol. 398, pp. 83–90, 2018.

[7] L. Qin, D. Bian, Y. Zhao, X. Xu, and Y. Guo, "Study on the preparation and mechanical properties of alumina ceramic coating reinforced by graphene and multi-walled carbon nanotube," *Russian Journal of Applied Chemistry*, vol. 90, no. 5, pp. 811–817, 2017.

[8] L. Jin, Y. Zeng, L. Xia, and Y. Ye, "Experimental and numerical investigation of mechanical behaviors of cemented soil–rock mixture," *Geotechnical & Geological Engineering*, vol. 35, no. 1, pp. 1–18, 2016.

[9] P. Shan and X. Lai, "Influence of CT scanning parameters on rock and soil images," *Journal of Visual Communication and Image Representation*, vol. 58, no. 1, pp. 642–650, 2019.

[10] P. Shan and X. Lai, "Mesoscopic structure PFC~2D model of soil rock mixture based on digital image," *Journal of Visual Communication and Image Representation*, vol. 58, pp. 407–415, 2019.

[11] H. Xing, L. Liu, and Y. Luo, "Water-induced changes in mechanical parameters of soil-rock mixture and their effect on talus slope stability," *Geomechanics and engineering*, vol. 18, no. 4, pp. 353–362, 2019.

[12] M. Gao, H. Wang, Y. Wang, T. Shen, and W. Wu, "Flame retardancy and mechanical properties of a novel intumescent flame- retardant unsaturated polyester," *Journal of Vinyl and Additive Technology*, vol. 22, no. 3, pp. 350–355, 2016.

[13] X. H. Yang, Y. P. Zhu, N. Guo, Z. B. Shi, and G. L. Ran, "Research on effects of compactness and matric suction on strength deformation characteristics of soil-rock aggregate mixture," *Rock and Soil Mechanics*, vol. 38, no. 11, pp. 3205–3214, 2017.

[14] J. Peranic and Z. Arbanas, "Impact of the wetting process on the hydro-mechanical behavior of unsaturated residual soil from flysch rock mass: preliminary results," *Bulletin of Engineering Geology and the Environment*, vol. 79, no. 2, pp. 985–998, 2020.

[15] H. Z. Wei, W. J. Xu, C. F. Wei, and Q. S. Meng, "Influence of water content and shear rate on the mechanical behavior of soil-rock mixtures," *SCIENCE CHINA Technological Sciences*, vol. 61, no. 8, pp. 1127–1136, 2018.

[16] W. Tun Tun, T. Sato, H. Saito, and Y. Kohgo, "Mechanical properties and stress–dilatancy relationships of unsaturated soil under various cyclic loading conditions," *Acta Geotechnica*, vol. 15, no. 7, pp. 1799–1813, 2020.

[17] H. Toyota, S. Takada, and A. Susami, "Rate dependence on mechanical properties of unsaturated cohesive soil with stress-induced anisotropy," *Soils and Foundations*, vol. 59, no. 4, pp. 1013–1023, 2019.

[18] H. Toyota, S. Takada, and A. Susami, "Mechanical properties of saturated and unsaturated cohesive soils with stress-induced anisotropy," *Geotechnique*, vol. 68, no. 10, pp. 883–892, 2018.

[19] P. B. Xu, H. Xu, and H. M. Wen, "3D meso-mechanical modeling of concrete spall tests," *International Journal of Impact Engineering*, vol. 97, pp. 46–56, 2016.

[20] Y. Li, Z. Guan, Z. Wang et al., "3D meso-scale finite element modelling on cement paste corroded in sodium sulfate with X-ray CT technique," *Construction and Building Materials*, vol. 202, pp. 727–737, 2019.

[21] J. Suchorzewski, J. Tejchman, M. Nitka, and J. Bobiński, "Meso-scale analyses of size effect in brittle materials using DEM," *Granular Matter*, vol. 21, no. 1, pp. 9–15, 2019.

[22] D. Ghosh and E. M. Constantinescu, "Well-balanced, conservative finite difference algorithm for atmospheric flows," *AIAA Journal*, vol. 54, no. 4, pp. 1370–1385, 2016.

[23] J. Hajrasouliha, R. J. Nedoushan, M. Sheikhzadeh, and T. Dastan, "Meso-macro numerical modeling of noncircular braided composite parts based on braiding process parameters," *Composite Structures*, vol. 224, p. 111065, 2019.

[24] J. Chen and L. Wang, "Mechanical parameters of wheat in triaxial compression tests and meso-mechanics simulation," *Journal of Computational and Theoretical Nanoscience*, vol. 13, no. 9, pp. 6387–6394, 2016.

[25] P. F. Shan, "Image segmentation method based on K-mean algorithm," *EURASIP Journal on Image and Video Processing*, vol. 2018, no. 1, 9 pages, 2018.

[26] M. Abdolmaleky, M. Naseri, J. Batle, A. Farouk, and L. H. Gong, "Red-green-blue multi-channel quantum representation of digital images," *Optik*, vol. 128, pp. 121–132, 2017.

[27] M. Márton, F. Markolt, L. Szabó et al., "Den site selection of the European badger,Meles melesand the red fox,Vulpes vulpesin Hungary," *Journal of Vertebrate Biology*, vol. 65, no. 1, pp. 72–79, 2016.

[28] G. Okuma, D. Kadowaki, Y. Shinoda, T. Akatsu, O. Guillon, and F. Wakai, "Determination of the size of representative volume element for viscous sintering," *Journal- Ceramic Society Japan*, vol. 124, no. 4, pp. 421–425, 2016.

[29] W. Kim and S. Y. Choi, "An improved implicit time integration algorithm: the generalized composite time integration algorithm," *Computers & Structures*, vol. 196, pp. 341–354, 2018.

[30] Z. Wang, B. Wu, G. Xu, and O. S. Bursi, "An improved equivalent force control algorithm for hybrid seismic testing of nonlinear systems," *Structural Control & Health Monitoring*, vol. 25, no. 2, 2018.

[31] J. Li and K. Yu, "An alternative to the Bathe algorithm," *Applied Mathematical Modelling*, vol. 69, no. MAY, pp. 255–272, 2019.

[32] S. Ma and H. Yuan, "A continuum damage model for multiaxial low cycle fatigue of porous sintered metals based on the critical plane concept," *Mechanics of Materials*, vol. 104, pp. 13–25, 2017.

[33] L. I. Jian, S. Chen, and L. Jiang, "On implicit integration of the bounding surface model based on swell-shrink rules," *Applied Mathematical Modelling*, vol. 40, no. 19-20, pp. 8671–8684, 2016.

[34] J. F. Chen and E. V. Morozov, "A consistency elasto-viscoplastic damage model for progressive failure analysis of composite laminates subjected to various strain rate loadings," *Composite Structures*, vol. 148, no. Jul., pp. 224–235, 2016.